Korean J. Chem. Eng., 37(8), 1365-1370 (2020)
DOI: 10.1007/s11814-020-0582-6

pISSN: 0256-1115
eISSN: 1975-7220

Confinement of Ru nanoparticles inside the carbon nanotube: Selectivity controls on methanol decomposition

Se-Won Park*, Ji Hoon Park*, Chang Won Yoon,†, and Jin Hee Lee*,†**

*Center for Environment and Sustainable Resources, Korea Research Institute of Chemical Technology, 141 Gajeong-ro, Daejeon 34114, Korea
**Center for Hydrogen Fuel Cell Research, Korea Institute of Science and Technology, 5 Hwarang-ro 14-gil, Seongbuk-gu, Seoul 02792, Korea
(*Received 19 March 2020 • Revised 14 May 2020 • Accepted 15 May 2020*)

Abstract−Carbon nanotubes (CNT) have been widely used as catalyst supports, and the confinement of metal nanoparticles inside the CNT cavity have received much attention. In this study, graphitic carbon nitride were used to introduce nitrogen to CNT and form ruthenium nanoparticles inside the CNT channel. The XPS evidenced that the ruthenium nanoparticles in the CNT cavity are present in more reduced state, and the nitrogen species are in a pyridinic and a pyrrolic form. The prepared catalysts exhibited excellent hydrogen and carbon monoxide selectivity. The hydrogen-to-carbon monoxide ratio was close to the stoichiometric ratio of methanol decomposition. In contrast, the ruthenium nanoparticles outside the CNT showed lower carbon monoxide selectivity at high methanol conversion. The alteration of electrical properties of ruthenium nanoparticles by the CNT channel and N-doping might hamper side reactions, such as water gas shift, methanation, dimethyl ether formation upon methanol decomposition.

Keywords: Nanoparticle Confinement, Methanol Decomposition, Syngas, Ruthenium, N-doped Carbon Nanotube

INTRODUCTION

Carbon nanotubes (CNT) have widely been utilized as catalyst supports, films, and electric materials owing to their high electric conductivity and robustness [1]. Recent studies demonstrated the distinctive properties of the confined metal nanoparticles inside the CNT cavity. Bao's research group reported the extremely enhanced ethanol production performance of rhodium based catalyst inside CNT [2]. A carbon monoxide binding mode and binding strength are altered by nanoparticle confinement in the CNT channel, which ultimately facilitates C-O bond dissociation and ethanol formation. Serp and co-workers delivered PtRu nanoparticles into the CNT using a specific ligand which has a high affinity to CNT [3]. This catalyst showed excellent performance on cinnamaldehyde hydrogenation attributes to the confinement of active sites and reactants in the CNT. Peralta-Inga et al. showed that the difference of charge distribution inside and outside of the nanotubes [4]. The theoretical results indicate that the difference in charge density could affect the adsorption of gas molecules. Su and co-workers reported nanoparticles inside the CNT have sintering resistance and show high durability on electrocatalytic applications [5].

Those attractive characteristics of the nanoparticles inside CNT have drawn huge attention and a number of methods have been developed to integrate nanoparticles into the CNT. The most common method is the impregnation of precursor solution to CNT, which relies only on the capillary force of CNT [6]. The stepwise fabrication method of nanoparticles in the CNT-nitrogen dope carbon interlayer was reported by Jiang's research group [7]. *In situ* synthetic approach of cobalt nanoparticles confined CNT structure was reported by Farrokhpour and co-workers.

Also, researches about methanol decomposition have been studied with various catalysts. Particularly, methanol decomposition can be catalyzed by numerous transition metals such as Pt, Pd, Rh, Co, Ni, Fe, and Mo [8-17]. However, high methanol conversion often leads to the selectivity loss due to the side reactions (Eq. (5)-(7)). CuO/SBA-15 showed >95% carbon monoxide selectivity at lower methanol conversion below 50%, but the carbon monoxide selectivity at 90% was lower than 80% [13]. Pt/$SrTiO_2$ catalyst exhibited <90% hydrogen selectivity in the all methanol conversion range [16].

Here we report a nitrogen doping induced localization of ruthenium nanoparticles inside the CNT channel. The g-C_3N_4 was employed to perform dual roles of a nitrogen doping agent on CNT and a nanoparticle delivering agent into the CNT channel. The ruthenium nanoparticles located inside and outside of the CNT exhibited distinguished physical and chemical properties. As results, different catalytic behaviors were demonstrated on hydrogen and carbon monoxide production during methanol decomposition.

EXPERIMENTAL

1. Catalyst Synthesis and Characterizations

All the chemicals were purchased from Sigma-Aldrich and used as received. For the synthesis of graphitic carbon nitride (g-C_3N_4), dicyandiamide was calcined at 550 °C for 4 h under static air to give a brownish-yellow powder. For the synthesis of Ru-NCNT,

†To whom correspondence should be addressed.
E-mail: cwyoon@kist.re.kr, leejh@krict.re.kr

which is ruthenium nanoparticles in nitrogen doped CNT, ruthenium chloride hydrate (0.50 g), multi-walled carbon nanotube (1.0 g), graphitic carbon nitride (g-C_3N_4, 1.0 g) were mixed in deionized water (50 mL). The mixture was sonicated for 10 min at room temperature and heated at 100 °C for 4 h under vigorous stirring to evaporate water. The resulting black solid was ground and treated at 550 °C for 4 h under nitrogen flow to give Ru-NCNT as a black powder. The identical procedure was followed for the synthesis of Ru-CNT, which is ruthenium nanoparticles on CNT, except that g-C_3N_4 was not used.

The prepared catalysts were analyzed by X-ray diffraction (XRD), transmission electron microscope (TEM), and X-ray photoelectron spectroscopy (XPS). XRD was recorded on a Rigaku Mini Flex II with Cu K_α radiation (λ=1.54 Å). TEM images were obtained using a Philips CM30 at 200 kV. XPS was implemented on a Thermo VF scientific, K_α.

2. Catalytic Activity Evaluation

Catalytic methanol decomposition was performed in a fixed-bed reactor using 0.10 g of catalyst shaped to 150-300 mm. The catalyst was pre-reduced at 250 °C for 2 h under 10% H_2/N_2 flow. Methanol was fed into the evaporator with 30 μL·min^{-1}, then delivered to the reactor with 50 mL·min^{-1} of nitrogen as carrier gas. The calculated methanol concentration was 29 vol% and the space velocity was 666 mL·(min·g_{cat})$^{-1}$. The reaction was performed between 250 to 550 °C and product gases were monitored by online gas chromatography (GC, Agilent).

Methanol conversion, carbon monoxide selectivity, and hydrogen selectivity were calculated with Eqs. (1)-(3).

$$\text{MeOH conversion (\%)} = \frac{\text{Sum of all carbon proudcts (mmol)}}{\text{Amount of MeOH (mmol)}} \times 100 \quad (1)$$

$$\text{Carbon monoxide selectivity (\%)} = \frac{\text{Amount of CO in product gases (mmol)}}{\text{Amounts of all carbon products (mmol)}} \times 100 \quad (2)$$

$$\text{Hydrogen selectivity (\%)} = \frac{\text{Amounts of } H_2 \text{ in product gases (mmol)}/2}{\text{Amounts of reacted Methanol (mmol)}} \times 100 \quad (3)$$

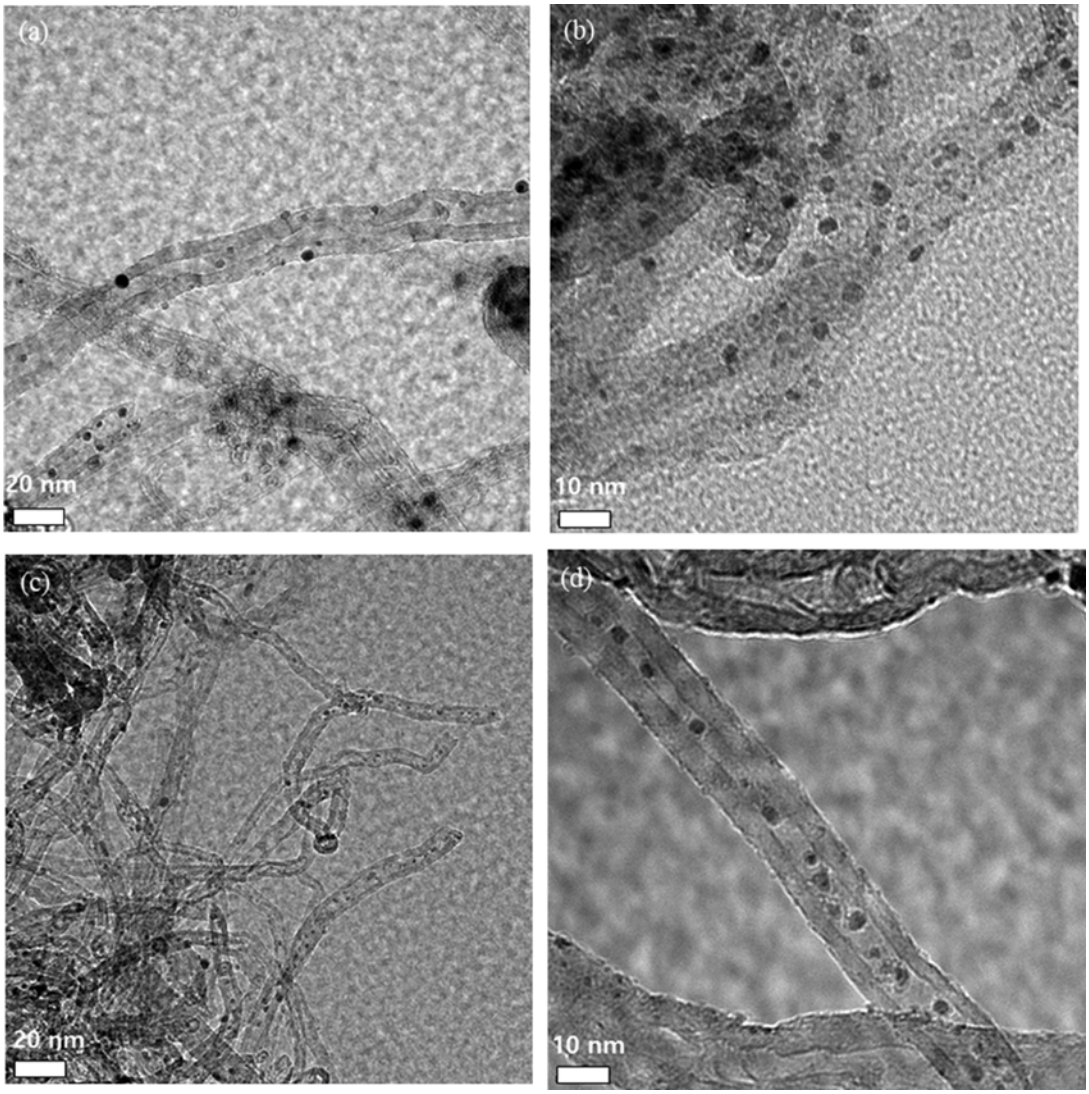

Fig. 1. TEM images of fresh catalysts. (a), (b) for Ru-CNT, (c), (d) for Ru-NCNT.

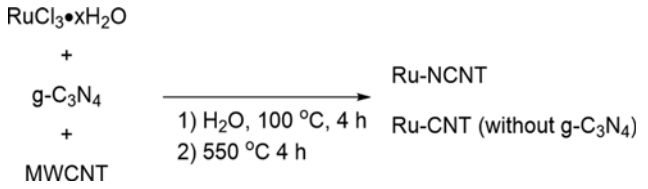

Scheme 1. Synthesis of Ru-CNT and Ru-NCNT.

RESULTS AND DISCUSSION

1. Physical Properties of the Catalysts

Nitrogen doping of CNT was accomplished using g-C_3N_4. g-C_3N_4 has a good nitrogen doping ability to carbon based material because g-C_3N_4 has plenty of nitrogen atoms (61 wt% N, based on chemical formula) and has fully conjugated sp^2 structure, which enables π-π interaction with carbon materials such as CNT, activated carbon, and graphene [18,19]. Ru-CNT and Ru-NCNT were prepared by wet-impregnation of ruthenium chloride, MWCNT, and w/ or w/o g-C_3N_4 (Scheme 1).

The TEM images of catalysts indicates the formation of 2-5 nm sized ruthenium nanoparticles both in Ru-CNT and Ru-NCNT. The g-C_3N_4 did not affect the particle size of the final catalysts (Fig. 1). A clear difference was found in the location of ruthenium nanoparticles. The ruthenium nanoparticles of Ru-CNT were deposited along the surface of CNT (Fig. 1(a)-(b)), while the ruthenium nanoparticles of Ru-NCNT were mainly located inside the CNT channel (Fig. 1(c)-(d)). These results indicate that the g-C_3N_4 induces nanoparticle formation inside the CNT channel. The nitrogen atoms in g-C_3N_4 have high affinity to metallic cation [20], and sp^2 conjugated structure of g-C_3N_4 favors π-π interaction with CNT. Thus, g-C_3N_4 could effectively deliver ruthenium cations into the CNT channel during the catalyst synthesis process. While the impregnation of aqueous solution into the CNT channel might not preferred without g-C_3N_4 due to hydrophobic characteristic of CNT.

Fig. 2 shows XRD patterns of Ru-CNT and Ru-NCNT. Both catalysts show broad and characteristic diffraction patterns of the carbon material at 2θ=27° and 45° (JCPDS 75-2078), which is attributed to carbon-carbon stacking structure [21]. Small ruthenium diffraction peaks appear at 2θ=38.39° and 69.41° of Ru-NCNT XRD pattern (JCPDS 06-0996). The ruthenium diffraction peak intensity of Ru-NCNT is higher than that of Ru-CNT. This indicates that the crystal domain size of Ru-NCNT is larger than that of Ru-CNT. However, it cannot be directly related to the nanoparticle size of Ru-CNT and Ru-NCNT due to the low intensity. As evidenced by TEM analyses, the particle size of two catalysts is almost similar.

XPS was measured to elucidate the electronic structure of the ruthenium, carbon, and nitrogen species in the catalysts. The Ru 3p spectra were deconvoluted to metallic ruthenium at 461 eV and ruthenium (IV) oxide at 463 eV [22-24] (Fig. 3). The spectra displayed that the Ru-NCNT exists in a more reduced state. The Ru(0)/Ru(IV) ratios are 2.19 and 4.55 for Ru-CNT and Ru-NCNT, respectively. Because lone pair electrons in nitrogen atoms make CNT more electronegative, the ruthenium nanoparticles in the N-doped CNT are more reducible than ruthenium nanoparticles in

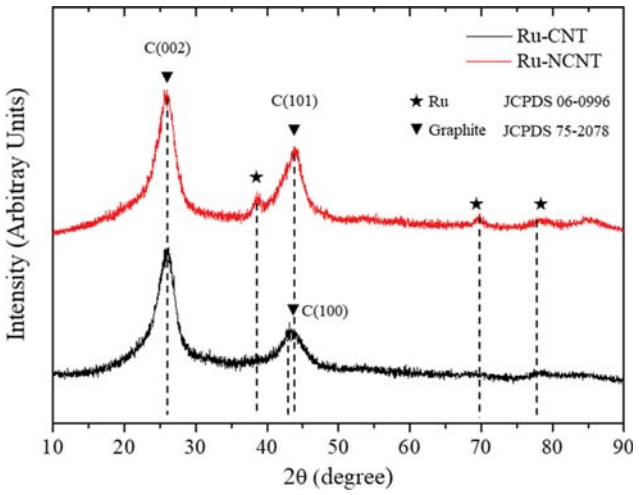

Fig. 2. XRD patterns of Ru-CNT and Ru-NCNT.

normal CNT. The different electronic environment inside and outside of the CNT affects the reducibility of ruthenium nanoparticles as well. The deconvoluted C1s XPS of Ru-CNT and Ru-NCNT showed a sharp C=C peak at 284.21 eV, a small C-C peak at 285.23 eV, and a C-O peak at 285.99 eV [25,26]. C=C peak is a major peak which constitutes the CNT frame. The defect sites of CNT, which could be enhanced by N-doping, are attributed to C-C peak; the Ru-NCNT thus occupies higher portions of C-C bonds (Fig. 3(c)-(d)). The pyridinic and pyrrolic N centered at 398 eV and 400 eV, respectively, were predominant in the N1s XPS spectra of Ru-NCNT [27-29].

2. Methanol Decomposition

Ru-CNT and Ru-NCNT were employed as catalysts for methanol decomposition. Methanol is the simplest alcohol compound which produces carbon monoxide and hydrogen upon decomposition. Methanol decomposition includes several unwanted pathways, such as water gas shift (WGS), methanation, dimethylether formation [30,31] (Eq. (5)-(7)); thus, selectivity control is pivotal to yield more hydrogen and carbon monoxide.

$$CH_3OH \rightarrow CO + 2H_2 \quad (4)$$

$$2CH_3OH \rightarrow H_3COCH_3 + H_2O \quad (5)$$

$$CO + H_2O \rightarrow CO_2 + H_2 \quad (6)$$

$$CO + 3H_2 \rightarrow CH_4 + H_2O \quad (7)$$

Fig. 4(a)-(b) shows methanol conversion and carbon monoxide selectivity of methanol decomposition catalyzed by Ru-CNT and Ru-NCNT. As temperature increases, the methanol conversion increases over both Ru-CNT and Ru-NCNT catalysts. Ru-CNT exhibited a higher methanol conversion than Ru-NCNT below 500 °C, but the catalytic activity over 550 °C was higher on Ru-NCNT. These results indicate that the nanoparticles outside the CNT exhibit higher catalytic activity toward methanol decomposition, likely due to easier accessibility of reactant methanol to the more exposed surface sites than inside the channel. In contrast, the trend of carbon monoxide selectivity was different from methanol conversion. The car-

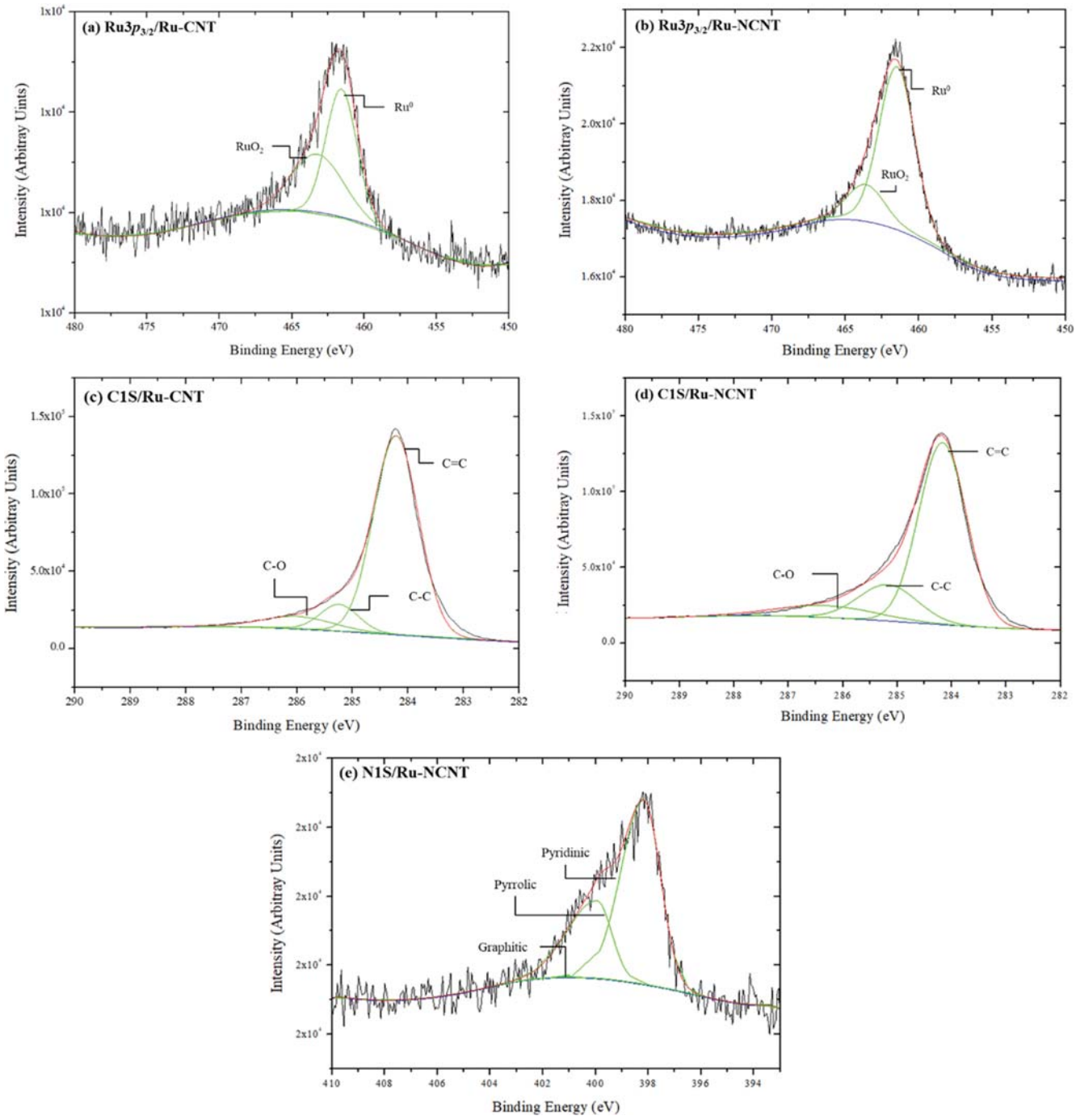

Fig. 3. Ru3p, C1S, and N1S XPS spectra of Ru-CNT and Ru-NCNT.

bon monoxide selectivity of methanol decomposition catalyzed by Ru-CNT reached the peak value at 400 °C, then significantly decreased over 400 °C. However, carbon monoxide selectivity of Ru-NCNT was >99% in the entire temperature range. Both methanol conversion and carbon monoxide selectivity reached >95% at 550 °C on Ru-NCNT. These results signify that the side reactions which produce other products than carbon monoxide occur on Ru-CNT at high temperature. The different reaction pathways in Ru-CNT and Ru-NCNT are evident from product gas distributions (Fig. 4(c)-(d)). Significant amounts of carbon dioxide and methane were produced on Ru-CNT over 400 °C. On the other hand, hydrogen and carbon monoxide were exclusively formed on Ru-NCNT.

Hydrogen to carbon monoxide ratios of Ru-NCNT over 300 °C are close to stoichiometric ratio of methanol decomposition (Fig. 5(a)). This result again clarifies that Ru-NCNT exclusively catalyzes methanol decomposition, and other reactions, such as WGS, and methanation, rarely occur on Ru-NCNT. In contrast, hydrogen to carbon monoxide ratios of Ru-CNT increase from 1.8 to 2.5 as temperature increases from 250 °C to 500 °C because WGS uti-

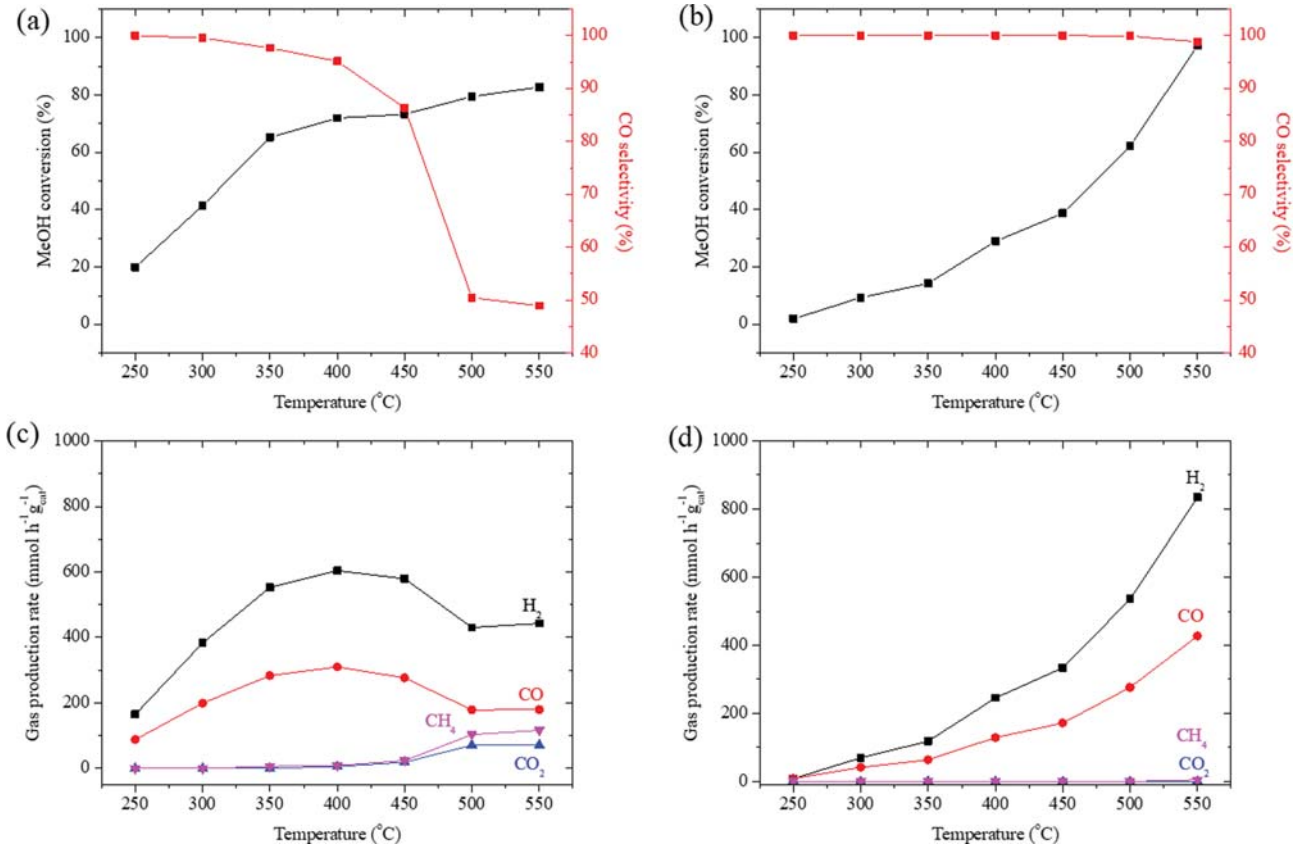

Fig. 4. Methanol decomposition profiles. Methanol conversion and carbon monoxide selectivity catalyzed by (a) Ru-CNT, (b) and Ru-NCNT. Product gas distributions catalyzed by (c) Ru-CNT, and (d) Ru-NCNT.

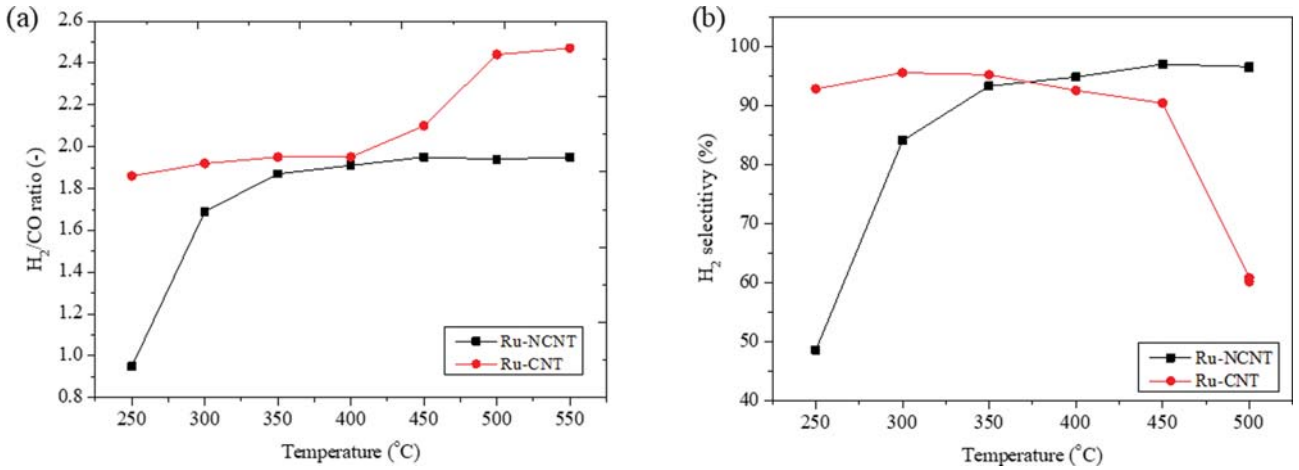

Fig. 5. (a) Hydrogen to carbon monoxide ratios, and (b) hydrogen selectivity on methanol decomposition catalyzed by Ru-CNT and Ru-NCNT.

lizes one molecule of carbon monoxide and produces one molecule of hydrogen. Hydrogen selectivity plot supports as well the selective methanol decomposition on Ru-NCNT over 350 °C (Fig. 5(b)).

As shown by other reports [13,16], methanol conversion and hydrogen selectivity are in a trade-off relation on Ru-CNT. However, hydrogen selectivity is higher on Ru-NCNT regardless of methanol conversion (Fig. 4 and 5). These results indicate that active sites of Ru-NCNT catalyze methanol decomposition but are not active other for reactions such as WGS and carbon monoxide methanation. The highly selective catalysis of Ru-NCNT might due to the low activity of Ru-NCNT toward carbon monoxide, which is attributed to electrical alteration by N-doping and nanoparticle confinements [32,33].

CONCLUSION

Ruthenium nanoparticles were introduced into the CNT channel via g-C_3N_4 induced nanoparticle formation. The ruthenium species in Ru-NCNT is in more reduced state than ruthenium species in Ru-CNT. Those electrical adjustments might due to the different electrical environments inside and outside of CNT and nitrogen doping effects. Methanol decomposition catalyzed by Ru-CNT, ruthenium nanoparticle outside of CNT, and Ru-NCNT, ruthenium nanoparticles inside of CNT, showed a clearly different catalytic performance. Ru-NCNT exhibited extraordinary hydrogen and carbon monoxide selectivity in methanol decomposition. The catalytic active sites of Ru-NCNT seem inert on WGS, carbon monoxide methanation in all temperature range. The stoichiometric formation of hydrogen and carbon monoxide also displays high selectivity of Ru-NCNT. Our study provides a novel method for nanoparticle confinement in CNT and the possibility of catalytic pathway control using confined nanoparticles.

ACKNOWLEDGEMENT

This research was financially supported by the National Research Foundation of Korea (NRF-2019M3E6A1064910).

REFERENCES

1. D. Zhang, G. Wei, Y. Wang, J. Wang, P. Ning, Q. Zhang, M. Wang, T. Zhang and K. Long, *Korean J. Chem. Eng.*, **35**(10), 1979 (2018).
2. X. Pan, Z. Fan, W. Chen, Y. Ding, H. Luo and X. Bao, *Nat. Mater.*, **6**(7), 507 (2007).
3. E. Castillejos, P.-J. Debouttière, L. Roiban, A. Solhy, V. Martinez, Y. Kihn, O. Ersen, K. Philippot, B. Chaudret and P. Serp, *Angew. Chem. Int. Ed.*, **48**(14), 2529 (2009).
4. Z. Peralta-Inga, P. Lane, J. S. Murray, S. Boyd, M. E. Grice, C. J. O'Connor and P. Politzer, *Nano Lett.*, **3**(1), 21 (2003).
5. H. Liu, L. Zhang, N. Wang and D. S. Su, *Angew. Chem. Int. Ed.*, **53**(46), 12634 (2014).
6. J.-P. Tessonnier, L. Pesant, G. Ehret, M. J. Ledoux and C. Pham-Huu, *Appl. Catal. A: Gen.*, **288**(1), 203 (2005).
7. D. Wang, J. Liu, J. Xi, J. Jiang and Z. Bai, *Appl. Surf. Sci.*, **489**, 477 (2019).
8. I. Palacio and O. R. de la Fuente, *Surf. Sci.*, **606**(15-16), 1152 (2012).
9. J. Sieben and M. Duarte, *Int. J. Hydrogen Energy*, **37**(13), 9941 (2012).
10. R. Shiozaki, T. Hayakawa, Y.-y. Liu, T. Ishii, M. Kumagai, S. Hamakawa, K. Suzuki, T. Itoh, T. Shishido and K. Takehira, *Catal. Lett.*, **58**(2-3), 131 (1999).
11. S. Hokenek and J. N. Kuhn, *ACS Catal.*, **2**(6), 1013 (2012).
12. D. Paneva, T. Tsoncheva, E. Manova, I. Mitov and T. Ruskov, *Appl. Catal. A: Gen.*, **267**(1-2), 67 (2004).
13. T. Tsoncheva, I. Genova, M. Stoyanova, M.-M. Pohl, R. Nickolov, M. Dimitrov, E. Sarcadi-Priboczki, M. Mihaylov, D. Kovacheva and K. Hadjiivanov, *Appl. Catal. B: Environ.*, **147**, 684 (2014).
14. M. Fan, Y. Xu, J. Sakurai, M. Demura, T. Hirano, Y. Teraoka and A. Yoshigoe, *Catal. Lett.*, **144**(5), 843 (2014).
15. S. Hong and T. S. Rahman, *J. Am. Chem. Soc.*, **135**(20), 7629 (2013).
16. H. Wang, J. Lu, C. L. Marshall, J. W. Elam, J. T. Miller, H. Liu, J. A. Enterkin, R. M. Kennedy, P. C. Stair and K. R. Poeppelmeier, *Catal. Today*, **237**, 71 (2014).
17. G. Marbán, A. López, I. López and T. Valdés-Solís, *Appl. Catal. B: Environ.*, **99**(1-2), 257 (2010).
18. J. H. Lee, M. J. Park, S. J. Yoo, J. H. Jang, H.-J. Kim, S. W. Nam, C. W. Yoon and J. Y. Kim, *Nanoscale*, **7**(23), 10334 (2015).
19. T. N. Hien, Y. H. Kim, M. Jeon, H. J. Lee, M. Ridwan, R. Tamarany and W. C. Yoon, *Materials*, **8**(6), 3442 (2015).
20. J. H. Lee, J. Ryu, J. Y. Kim, S.-W. Nam, J. H. Han, T.-H. Lim, S. Gautam, K. H. Chae and C. W. Yoon, *J. Mater. Chem. A*, **2**(25), 9490 (2014).
21. Y. K. Kim and H. Park, *Energy Environ. Sci.*, **4**(3), 685 (2011).
22. Y. Park, B. Lee, C. Kim, Y. Oh, S. Nam and B. Park, *J. Mater. Res.*, **24**(9), 2762 (2009).
23. Y. Qiao, S. Guo, K. Zhu, P. Liu, X. Li, K. Jiang, C.-J. Sun, M. Chen and H. Zhou, *Energy Environ. Sci.*, **11**(2), 299 (2018).
24. W.-J. Lee, S. Jeong, H. Lee, B.-J. Kim, K.-H. An, Y.-K. Park and S.-C. Jung, *Korean J. Chem. Eng.*, **34**(11), 2993 (2017).
25. R. Sadri, M. Hosseini, S. N. Kazi, S. Bagheri, N. Zubir, K. H. Solangi, T. Zaharinie and A. Badarudin, *J. Colloid Interface Sci.*, **504**, 115 (2017).
26. M.-H. Chen, C.-Y. Ke and C.-L. Chiang, *J. Compos. Sci.*, **2**(2), 18 (2018).
27. Z.-H. Sheng, L. Shao, J.-J. Chen, W.-J. Bao, F.-B. Wang and X.-H. Xia, *ACS Nano*, **5**(6), 4350 (2011).
28. J. H. Lee, M. J. Park, J. Jung, J. Ryu, E. Cho, S.-W. Nam, J. Y. Kim and C. W. Yoon, *Inorg. Chim. Acta*, **422**, 3 (2014).
29. J. Deng, P. Ren, D. Deng, L. Yu, F. Yang and X. Bao, *Energy Environ. Sci.*, **7**(6), 1919 (2014).
30. B. A. Sexton, *Surf. Sci.*, **102**(1), 271 (1981).
31. A. S. Moura, J. L. C. Fajín, A. S. S. Pinto, M. Mandado and M. N. D. S. Cordeiro, *J. Phys. Chem. C*, **119**(49), 27382 (2015).
32. G.-F. Wei, C. Shang and Z.-P. Liu, *Phys. Chem. Chem. Phys.*, **17**(3), 2078 (2015).
33. Z. Peralta-Inga, P. Lane, J. S. Murray, S. Boyd, M. E. Grice, C. J. O'Connor and P. Politzer, *Nano Lett.*, **3**(1), 21 (2003).